S. Müftü

Massachusetts Institute of Technology,
Haystack Observatory,
Westford, MA 01886
Assoc. Mem. ASME

T. S. Lewis

Eastman Kodak Company,
Engineering Research Center,
901 Elmgrove Road,
Rochester, NY 14653

K. A. Cole

Eastman Kodak Company,
Web Dynamics Group,
Building 10, Kodak Park,
Rochester, NY 14652

R. C. Benson

Professor and Head of Mechanical
Engineering,
Department of Mechanical Engineering,
The Pennsylvania State University,
University Park, PA 16802
Mem. ASME

A Two-Dimensional Model of the Fluid Dynamics of an Air Reverser

A theoretical analysis of the fluid mechanics of the air cushion of the air reversers used in web-handling systems is presented. A two-dimensional model of the air flow is derived by averaging the equations of conservation of mass and momentum over the clearance between the web and the reverser. The resulting equations are Euler's equations with nonlinear source terms representing the air supply holes in the surface of the reverser. The equations are solved analytically for the one-dimensional case and numerically for the two-dimensional case. Results are compared with an empirical formula and the one-dimensional air-jet theory developed for hovercraft. Conditions that maximize the air pressure supporting the web are analyzed and design guidelines are deduced.

1 Introduction

Products such as photographic film and paper are made and processed in continuous sheets known as webs. During these operations a web follows a complicated path over, under, and around various rollers, coaters, driers, and other devices. Air reversers are used in this path to change the moving direction of a coated wet web without touching it. As shown in Fig. 1, an air reverser is a large diameter hollow drum with holes in its surface. Air is pumped through these holes to create an air cushion on top of which the web can float. No contact is permitted between the web and the surface of the air reverser. The pressure distribution in the clearance between the web and the air reverser is determined by the size and distribution of the holes and the pressure inside the drum. In order to design air reversers that achieve adequate web flotation with minimum air flow, it is desirable to develop a theoretical model of the system.

Other applications of using an air cushion to float materials include externally pressurized bearings used in tape conveyance, air film conveyors used in transport of packages, and hovercraft. Even though the end result in these applications is to separate two surfaces, different hydrodynamic effects are at work. For example, at low operating clearances on the order of microns, common to tape and package conveyance, viscous forces dominate the air pressure generation. (Chandra et al., 1990; Gross, 1980, Chapter 6.5). On the other hand, in the air jet of a hovercraft, where the clearance is on the order of centimeters, the inertial forces are more important (Elsley and Devereux, 1968). In the former situation the air flow is commonly represented by the Reynolds equation and in the latter

situation by Euler's equations. See Gross (1980, Chapter 5) for more on the classification of the externally pressurized interfaces. The ratio of the inertial to viscous forces in a narrow channel, given by the modified Reynolds number $\text{Re}^* = \rho U h^2 / \mu L$, is a good measure of which approach should be taken. In the definition of Re^*, ρ is the density and μ is the viscosity of the fluid, U is a speed representative of the flow, h is the clearance height, and L is a scale length in the flow field (Hamrock, 1994).

The weight of a hovercraft is balanced by the "cushion pressure" generated by the airjet(s) placed on the skirt of the vehicle. Analytical expressions for this pressure can be found in Elsley and Devereux (1968) for the incompressible case and in Pozzi et al. (1993) for the compressible case. An air reverser usually has a complicated hole pattern as shown in Fig. 1 and in general the flow is two-dimensional in the plane of the web. Therefore the expressions developed for the hovercraft has limited use only for air-reversers with a specific hole pattern. Here we report on the general equations governing the two-dimensional air flow in an air cushion without any restrictions on the hole pattern.

In this paper we assume that the location of the web is fixed and known. The coupling between a flexible moving web and the air flow will be presented later. The equations governing the air flow are Euler's equations for momentum balance and the mass continuity equation, both with nonlinear source terms representing the holes. These equations are averaged over the spacing between the web and the reverser to obtain a two-dimensional model of the air flow in the plane of the web. An analytical solution of these equations can be found for the one-dimensional case with a constant gap height. The two-dimensional case is solved numerically.

2 Governing Equations

A balance of the forces acting on a membrane-like web requires that the air pressure p and the "belt-wrap" pressure $T/(RL_y)$ be in equilibrium (Müftü and Benson, 1996). Here T is
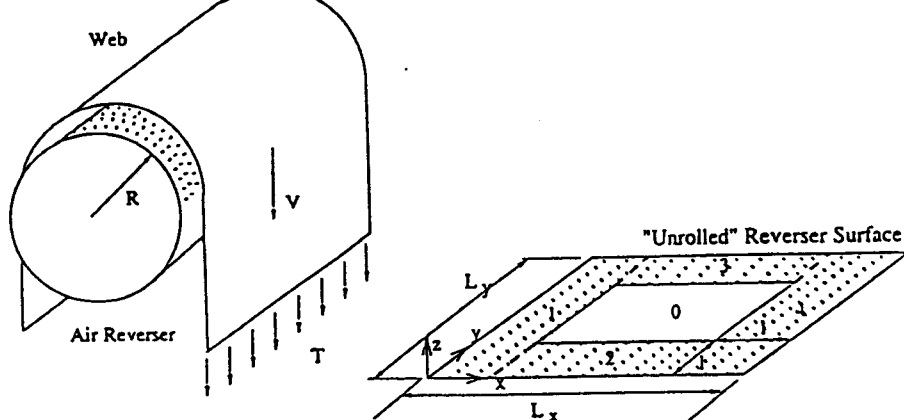
Fig. 1 Schematic view of a web moving over an air reverser under tension T and with speed V

the web tension, R is the reverser radius, and L_y is the web width, as shown in Fig. 1. For the typical values $R = 0.25$ m, $L_y = 1.5$ m, and $T = 200$ N, the pressure required to support the web is approximately $p = 533$ Pa.

The supply pressure inside the air reverser is typically $p_0 = 800$ Pa. The velocity U through one of the holes of the air reverser can be estimated from Bernoulli's equation

$$p + \tfrac{1}{2}\rho U^2 = p_0, \quad \text{or} \quad U = (2(p_0 - p)/\rho)^{1/2}, \quad (1)$$

where ρ is the density of air, which is 1.2 kg/m^3 at room conditions (Gerhart et al., 1992). For $p_0 - p = 267$ Pa, this gives $U = 21$ m/s. Velocities throughout the flow field are generally of the same order of magnitude as U. The gap between the web and the surface of the reverser is typically about 4 mm. Using $L_x = 0.8$ m as the length scale we find Re* = 14.5. This indicates that inertial forces dominate over viscous forces. Moreover, the fact that the Reynolds number Re $= \rho U h/\mu$ is 5450 indicates that the flow is turbulent ($\mu = 1.85 \times 10^{-5}$ Nsm^{-2}). Therefore, it is concluded that the effect of viscosity on pressure is negligible in the air reverser flow.

The diameter of the air reverser is large enough to make centrifugal effects negligible in the flow, so the cylindrical geometry of the problem can be unrolled onto a plane, as shown in Fig. 1. Here the x-axis is along the circumferential direction, the y-axis is along the axial direction, and the z-axis is perpendicular to the surface of the reverser. The flow field covers a rectangular region in the xy-plane. The web travels in the $+x$ direction, but its velocity (~ 2 m/s) is generally small compared to the velocity of the air under the web.

We assume that the clearance h between the web and the air reverser is small enough that the air flow can be considered two-dimensional. We thus neglect the velocity in the z direction and assume that the pressure p and the velocities u and v in the x and y directions, respectively, are functions of x and y but not z. The assumption of two-dimensional flow is not valid in the vicinity of each of the holes, but the details of the flow near the holes should not be important if the net effect of the mass and momentum flux through the holes is estimated correctly.

We assume that the holes in the reverser surface are sufficiently close together that they can be considered a uniform, distributed flow source. They can then be described by a single parameter α, the ratio of the total cross-sectional area of the holes to the total surface area. For circular holes of radius r_h arranged in a rectangular pattern with spacings b and c, as shown in Fig. 2(a), we have $\alpha = \pi r_h^2/bc$. At different parts of the reverser the hole density may be different. If there are no holes, $\alpha = 0$.

The equations describing the flow field can be derived by averaging the equations of conservation of mass and momentum over the clearance between the air reverser and the web

(Lewis). We also assume that the flow is incompressible and neglect viscous forces. This gives

$$\frac{\partial h}{\partial t} + \frac{\partial hu}{\partial x} + \frac{\partial hv}{\partial y} = \alpha U \qquad (2a)$$

$$\rho \frac{\partial u}{\partial t} + \rho u \frac{\partial u}{\partial x} + \rho v \frac{\partial u}{\partial y} + \frac{\partial p}{\partial x} = -\alpha \rho U \frac{u}{h} \qquad (2b)$$

$$\rho \frac{\partial v}{\partial t} + \rho u \frac{\partial v}{\partial x} + \rho v \frac{\partial v}{\partial y} + \frac{\partial p}{\partial y} = -\alpha \rho U \frac{v}{h}. \qquad (2c)$$

Equation (2a) is a form of the mass continuity equation with a source term αU. The terms on the right-hand sides of (2b) and (2c) represent the effect of the momentum flux through the holes. The pressure gradients created by these terms are
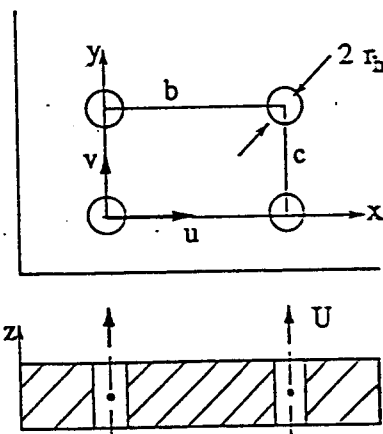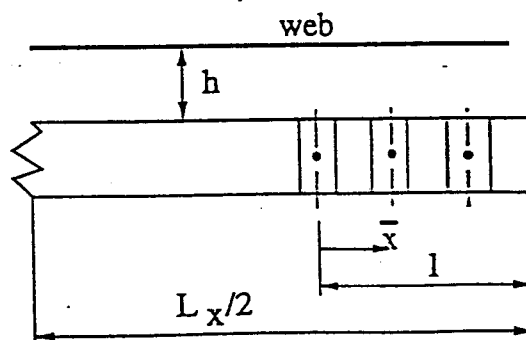

Fig. 2(a) Detail of the pressure holes

Fig. 2(b) One half of the one-dimensional problem

Fig. 2 Schematic view of the air reverser

proportional to the mass flow rate $\rho\alpha U$ and the local flow field velocities u and v.

In addition to Eqs. (2), it is necessary to specify the average velocity U through the holes. In general U is not constant, but varies from hole to hole and depends on the solution for the flow field. A reasonable first-order assumption is that U is a function of the pressure drop across the hole $p_0 - p$, where p_0 is the pressure inside the reverser (the supply pressure) and p is the local pressure under the web. In the absence of frictional losses, U would be given by Bernoulli's Eq. (1). If we assume that frictional losses are a fixed fraction of the original potential energy we get instead

$$U = \kappa(2(p_0 - p)/\rho)^{1/2} = \kappa U_0 (1 - p/p_0)^{1/2} \qquad (3)$$

where $U_0 = \sqrt{2p_0/\rho}$, and where κ is an empirical constant, lying between 0 and 1, which is commonly called the discharge coefficient. This equation is generally used in calculating the flow rate across the orifice of a flow measuring device; κ accounts for the losses due to turbulence and the contraction of the effective flow area near the orifice (Gerhart et al., 1992).

In our problem there is a more complicated mechanism for both momentum loss and exchange near a pressure hole. In the reverser gap the air jet coming through a hole is affected by both the web and the cross flow present in the gap, creating a very complicated three-dimensional flow. In general a wall, such as the web, placed in front of a jet stagnates the flow and hence causes pressure to rise (Rajaratnam, 1976, p. 231). If the jet velocity U is a function of the pressure drop across the hole then the presence of the web would reduce the average jet exit velocity. A different effect occurs in the presence of cross flow. When a jet is injected into a cross flow it locally retards the cross flow on the upstream side of the jet and causes rarefaction on the downstream side. Thus the pressure in the mixing fluid rises on the upstream side and drops on the down stream side. This pressure difference causes the jet to deflect (Abramovich, 1963, p. 542). Trying to approximate the combined interaction of these two effects by a single parameter κ is obviously an oversimplification, but it allows us to circumvent the solution of a very complicated three-dimensional problem. A separate and more detailed study of the discharge coefficient under the conditions described in this paragraph would be useful.

In an experiment without the web, the discharge coefficient for typical air reverser holes was estimated to be 0.65 (Lewis). If the gap between the web and the air reverser were large compared to the hole diameter, we would expect this value to be valid here. In practice, however, the gap is approximately equal to the hole diameter, which produces the complicated flow pattern described above, and makes it reasonable to expect that a different value may be appropriate. In fact, as will be seen later using a higher value of κ gives a closer match to empirically obtained pressures.

We assume that for most practical applications air will be flowing out of the web-reverser interface. Therefore we have an "outflow boundary" situation, where it is sufficient to prescribe only one boundary condition to obtain a well-posed boundary value problem (Fletcher, 1991). Indicating the outer periphery of the air reverser by B, we set the pressure to the ambient value

$$p = 0 \quad \text{on} \quad B. \qquad (4)$$

Note that p is given in terms of gauge pressure.

3 Analytical Solution

Some insight into the full two-dimensional problem can be obtained by considering a one-dimensional model. The one-dimensional model can be expected to be approximately correct

along and near the centerline of the web in either the x or y direction.

If we assume that the flow is only in the x direction, then the steady-state versions of Eqs. (2a) and (2b) become

$$\frac{d}{d\bar{x}}(hu) = \alpha U \qquad (5a)$$

$$\frac{dp}{d\bar{x}} + \rho u \frac{du}{d\bar{x}} + \frac{\rho\alpha U}{h} u = 0 \qquad (5b)$$

where U is again given by (3), and where $\bar{x}$ is a local coordinate for the region with sources, as shown in Figure 2(b). Equations (3) and (5) are still nonlinear, but if the clearance h between the air reverser and the web is constant, they can be solved exactly. In particular, substitution of (3) into (5a) gives

$$p = p_0 \left[1 - \left(\frac{h}{\kappa\alpha U_0} \frac{du}{d\bar{x}} \right)^2 \right]. \qquad (6)$$

Substitution of (3) and (6) into (5b) then gives the linear ordinary differential equation

$$\frac{d^2 u}{d\bar{x}^2} - 2\left(\frac{\kappa\alpha}{h} \right)^2 u = 0. \qquad (7)$$

The symmetrical air reverser shown in Fig. 2(b) contains two regions of width l with holes and a central region without holes. The total width of the web is L_x. By symmetry, the solutions for the regions on the left and right will be identical, and the solution for the central region will be given by $p =$ constant and $u = 0$. The appropriate boundary conditions for the region on the right are $u = 0$ at the edge of the central region $\bar{x} = 0$, and $p = 0$ at the edge of the web $\bar{x} = l$. Using these boundary conditions, the solution for the right-hand region can be found to be

$$u = U_0 \frac{\sinh(m\bar{x}/l)}{\sqrt{2}\cosh(m)} \qquad (8a)$$

$$p = p_0 \left[1 - \left(\frac{\cosh(m\bar{x}/l)}{\cosh(m)} \right)^2 \right] \qquad (8b)$$

where

$$m = \sqrt{2}\,\frac{\kappa\alpha l}{h}. \qquad (9)$$

The dimensionless parameter $\kappa\alpha l/h$ is the ratio of the effective area of the holes to the total exit area at the edge of the web. The higher this parameter, the more difficult it is for the flow to exit from under the web, and therefore the higher the pressure that is generated, as can be seen from Eq. (8b).

4 Numerical Solution

The full two-dimensional problem cannot be solved analytically. We used a numerical method, whose details can be found in Müftü et al. (1997), to solve the governing equations. This method employs a pseudo-transient iteration algorithm to calculate the steady-state solution where Eq. (2a) is replaced by

$$\frac{\partial ph}{\partial t} + \rho a^2 \left(\frac{\partial hu}{\partial x} + \frac{\partial hv}{\partial y} \right) = \rho a^2 \alpha U. \qquad (10)$$

In this equation a^2 is a constant which can be considered an artificial speed of sound (Fletcher, 1991, Vol. 2, p. 356). In this method the discrete time-step Δt which is introduced later and a^2 act like relaxation constants between the iterations.

During the solution iterations the air pressure p can sometimes become higher than the supply pressure p_0. When this occurs, the air velocity U is replaced by U^*;

$$U^* = \begin{cases} -\kappa(2|p_0 - p|/\rho)^{1/2} & \text{if } p > p_0 \\ \kappa(2|p_0 - p|/\rho)^{1/2} & \text{if } p_0 > p. \end{cases} \quad (11)$$

These sinks typically occur where two regions of substantially different hole densities α are placed close to each other. They disappear at steady state.

For convenience the following notation is used throughout this paper. The solution domain of the governing equation is indicated by $S = \{(x, y) : 0 \le x \le L_x \text{ and } 0 \le y \le L_y\}$ where x, y, L_x and L_y are as shown in Fig. 1. This domain is divided into two subdomains: $S = B \cup I$, where the inner domain is $I = \{(x, y) : 0 < x < L_x \text{ and } 0 < y < L_y\}$. The inner domain I is further subdivided into I_S where there are pressure sources and I_0 where there are no pressure sources. The boundary $B = B_1 \cup B_2 \cup B_3 \cup B_4$ is composed of the four edges:

$$B_1 = \{(x, y) : x = 0, 0 \le y \le L_y\},$$

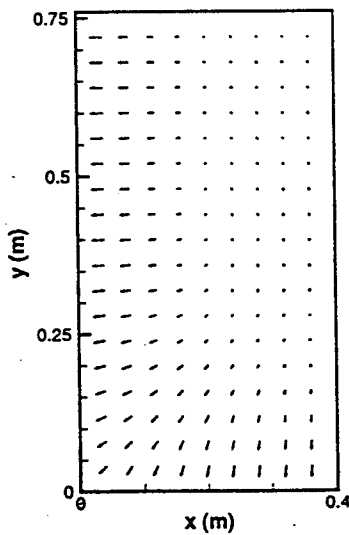$$B_2 = \{(x, y) : y = 0, 0 \le x \le L_x\},$$
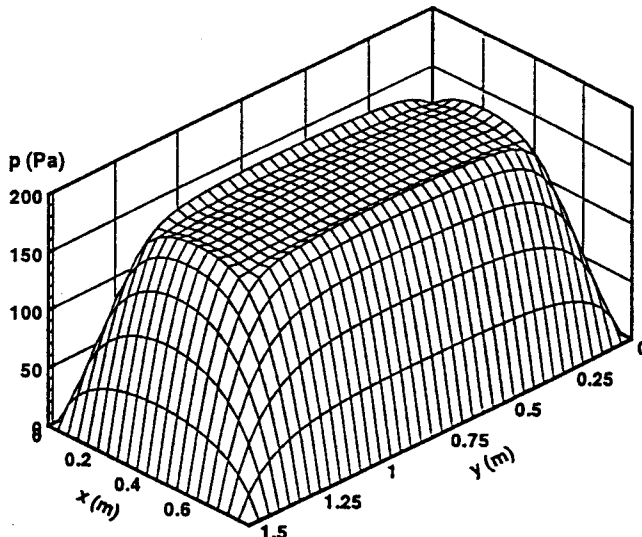
Fig. 3(a)   Air velocity vector, V

Fig. 3(b)   Air pressure distribution

Fig. 3   Air velocity and pressure profiles at steady state. Note that (a) shows only the lower left quarter of the solution domain; the solution is symmetrical with respect to $x = L_x/2$ and $y = L_y/2$ ($p_0 = 800$ Pa, $h_0 = 3$ mm, and $\alpha_{1-4} = 0.0084$).
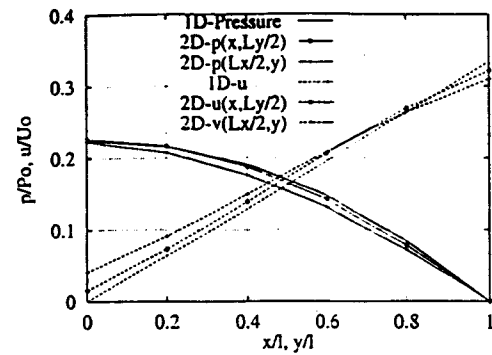
Fig. 4   Comparison of a one-dimensional analytical solution with two-dimensional numerical results ($\alpha_{1-4} = 0.0084$, $h_0 = 3$ mm, and $p_0 = 800$ Pa)

$$B_3 = \{(x, y) : y = L_y, 0 \le x \le L_x\},$$

$$B_4 = \{(x, y) : x = L_x, 0 \le y \le L_y\}.$$

The solution domain is discretized using a uniform rectangular mesh with $\Delta x = L_x/(M - 1)$ and $\Delta y = L_y/(N - 1)$ spacing between the nodes in the x and y directions, respectively, where M and N are the total number of discretization points along the x and y-axes. In I, Eqs. (2b, c) and (10) are discretized using second-order accurate central finite difference formulas. On B, velocities u and v are extrapolated from the inside solution and p is given by the pressure boundary condition (4).

Using the central finite difference formulas to discretize the governing equations uncouples the grid points in an odd-even fashion. This uncoupling causes an aliasing error (Hirsch, 1988, Vol. 1, p. 325). The aliasing is eliminated by adding artificial viscosity which transforms the discretized equations to an upwind equivalent formulation (Kwak et al., 1986). The artificial viscosity is provided by the following matrix operators, whose use is shown later in Eq. (14),

$$-[C_i]\{\Delta q^{n+1}\} = -\epsilon_i (L_{xx} \div L_{yy})\Delta q_k^{n+1} \quad (12a)$$

$$-[C_e]\{q^n\} = -\epsilon_e (L_{xxx} \div L_{yyy})q_k^n \quad (12b)$$

where q_k^n is one of the u, v, and p at current time level n and mesh point k, and $\Delta q_k^{n+1} = q_k^{n+1} - q_k^n$. The parameters ϵ_i and ϵ_e are the implicit and explicit artificial viscosity constants and the $[C_i]$ and $[C_e]$ are the matrix representation of the viscosity operators. For example in the y direction the difference operators are $L_{yyyy}u_k = (u_{k+2} - 4u_{k+1} + 6u_k - 4u_{k-1} + u_{k-2})$ and $L_{yy}u_k = (u_{k+1} - 2u_k + u_{k-1})$. Using $\epsilon_i = 2\epsilon_e$ leads to unconditional stability (Pulliam, 1985). On nodes adjacent to B the artificial viscosity is applied using special forms for Eqs. (12) (Müftü et al., 1997).

We use the Crank-Nicholson method, which provides an unconditionally stable time-stepping algorithm (Fletcher, 1991), for the discretizing Eqs. (10), (2b, c) in time. This gives, for example, for Eq. (2b),

$$\rho \frac{v_k^{n+1} - v_k^n}{\Delta t} + \frac{1}{2}(r_k^{(2)n+1} \div r_k^{(2)n}) = 0, \quad (13)$$

where $n + 1$ is the unknown time level, and Δt is the time-step size. The residuals $r^{(1)}$, $r^{(2)}$, and $r^{(3)}$ are obtained by collecting the time-independent terms of (10), (2b, c) on the left-hand side of the equations, respectively. The resulting equations are still nonlinear. They are linearized around a known time level t^n using Taylor series expansions.

After applying the time discretization, performing lineariza-

tion and adding the artificial viscosity operators given above, the system of equations can be represented in the following matrix form:

$$-\{R^n\} - [C_e]\{q^n\} = ([J^n] - [C_i])\{\Delta q^{n+1}\} \quad (14)$$

where $\{R^n\} = \{\{r^{(1)n}\}\{r^{(2)n}\}\{r^{(3)n}\}\}^T$, $\{\Delta q^{n+1}\} = \{\{\Delta u^{n+1}\}\{\Delta v^{n+1}\}\{\Delta p^{n+1}\}\}^T$, and $[J^n]$ is the Jacobian matrix. The bandwidth of the matrix $([J^n] - [C_i])$ is $3N$. This matrix is nonlinear, therefore it is inverted at every time step. We use the successive-over-relaxation method to solve (14). The solution advances in time by

$$\{q^{n+1}\} = \{q^n\} + \{\Delta q^{n+1}\}. \quad (15)$$

The solution process starts with zero initial conditions, $\{q^0\} = 0$.

5 Results

Typically the pressure holes are distributed around the outer edges of the air reverser, and there is a large area in the middle with no holes as shown in Fig. 1; in terms of the notation introduced before we have four inner regions with sources, I_{S1} – I_{S4}, and one sourceless inner region, I_0 marked "0." The physical dimensions of the air reverser considered here are $L_x = 0.8$ m, $L_y = 1.52$ m, and $l = 0.2$ m. The hole density α varies from 0.008 to 0.05, and the supply pressure p_o varies from 200 to 800 Pa. The discharge coefficient is $\kappa = 0.65$, and the spacing between the web and the air reverser has a constant value $h(x, y) = h_0 = 3$ mm unless otherwise stated in the figure captions. The values $a = 139$ m/s, $\Delta t = 10^{-3}$ s, $\epsilon_e = 2.5 \times 10^{-2}$, $M = 21$ and $N = 39$ along with the relation $\epsilon_i = 2\epsilon_e$ were used in all of the cases shown here, and were selected based on numerical experiments (Müftü et al., 1997).

5.1 Comparison of the One-Dimensional and the Two-Dimensional Solutions. Figure 3 shows a typical steady-state solution. In part (a) we give the air velocity vector, $V(x, y)$. In contrast to the one-dimensional analytical solution, where we assumed the air flow is zero at the inner edge of the source region, we make no assumptions about the flow conditions in I_0 in the numerical solution. Upon examining this figure we see that there is very little flow in I_0. Furthermore, the outflow from B is nearly uniform and perpendicular to each edge, thus approximately one-dimensional, except near the corner regions.

Figure 3(b) shows the two-dimensional air pressure profile corresponding to this case. Here we see that the pressure attains a constant value in the sourceless region, I_0, and in I_{S1-4} it gradually falls to ambient level on the outer edge, B. The pressure in the middle region is nearly uniform, and the one-dimensional assumption again seems to be valid, except near the corners of the reverser.
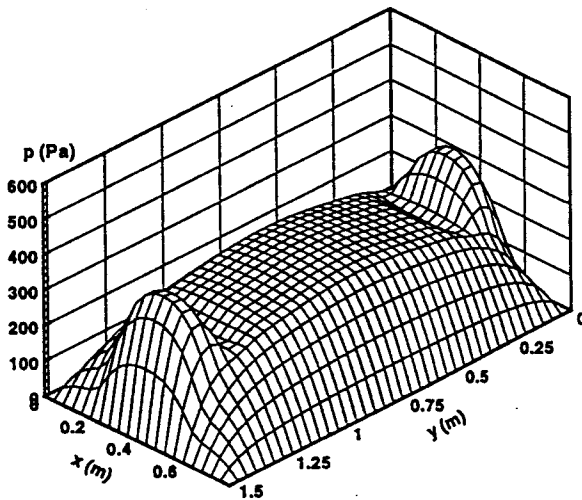

Fig. 5(a) $\alpha_{2,3} = 0.0252, \alpha_{1,4} = 0.0084$

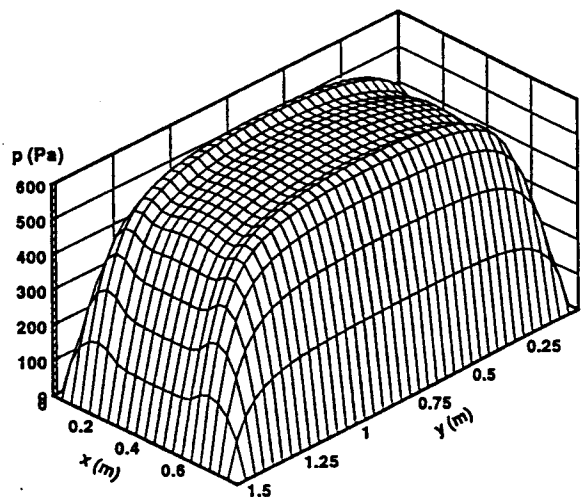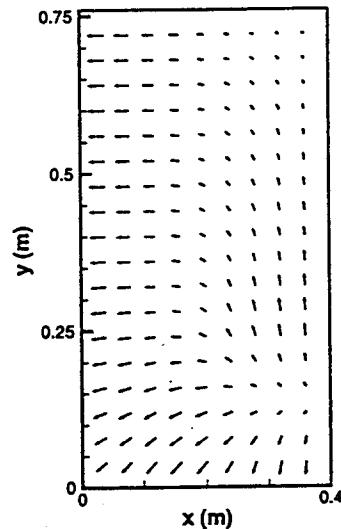
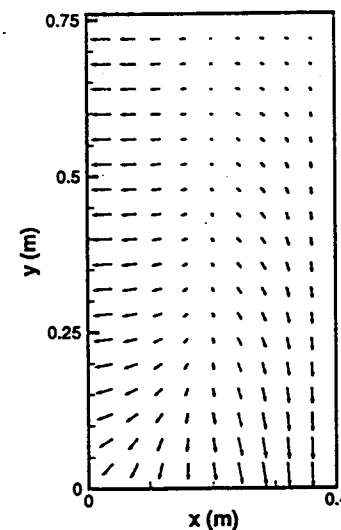Fig. 5(b) $\alpha_{2,3} = 0.0084, \alpha_{1,4} = 0.0252$

Fig. 5   The effect of hole density on the steady-state pressure profile ($h_0 = 3$ mm and $p_0 = 800$ Pa)

In Fig. 4 we compare the velocity profile from a one-dimensional solution with a calculated two-dimensional solution along the lines $\bar{x}$ in I_{s4} and $\bar{y}$ in I_{s2}. In general, the two-dimensional solution shows slightly higher velocities and lower pressures than the one-dimensional solution. The pressure profile in $\bar{x}$ is slightly higher than in $\bar{y}$. This is caused by the fact that I_{s4} has 3.8 times larger hole area (thus air in-flow) compared to I_{s2}.

5.2 Maximizing the Average Pressure. The air pressure distribution under the web can be changed by adjusting the source densities in regions I_{s1-4}. Figure 5 shows the effect of using different densities in different regions. When the source density is tripled in I_{s2} and I_{s3} with respect to the case shown in Fig. 3, the steady-state pressure takes the rather interesting distribution shown in Fig. 5(a). Here we see that the pressure in regions I_{s2} and I_{s3} reach a maximum of 355 Pa and in regions I_{s1} and I_{s4} a maximum of 300 Pa. On the other hand, if we use the one-dimensional assumption, then the pressure at the inner edge of a source region ($\bar{x} = 0$) given by (8b)

$$p_1 = p_0 \left[1 - \frac{1}{\cosh^2(m)} \right] \qquad (16)$$

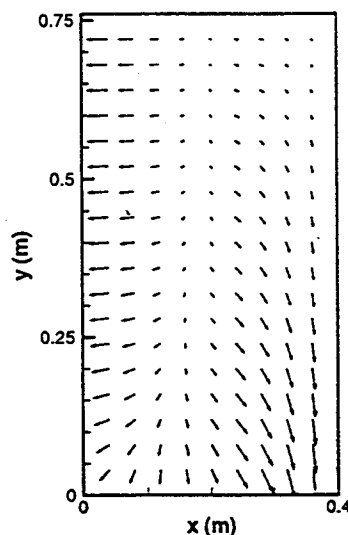would be 666 Pa ($m = 1.54$) and 179 Pa ($m = 0.51$) in $I_{s2,3}$.

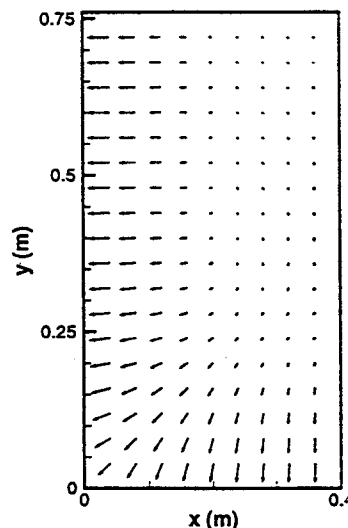Fig. 6(a) $\alpha_{2,3} = 0$, $\alpha_{1,4} = 0.0274$

Fig. 6(b) $\alpha_{1-4} = 0.0217$

Fig. 6 These two cases and the case shown in Fig. 7(b) have equivalent total hole area. The flow pattern and subsequently the pressure profile are greatly affected by the location and density of the holes (h_0 = 3 mm and p_0 = 800 Pa).
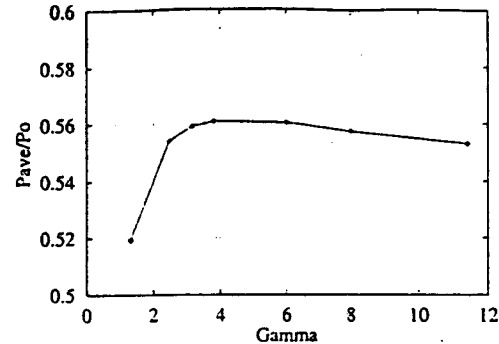
Fig. 7 The effect of the hole area ratio Γ = Gamma on the ratio P_{ave}/P_0 for a fixed total hole area of 0.0167 m^2. The maximum pressure occurs for a uniform α distribution (p_0 = 800 Pa, h_3 = 3 mm).

and $I_{s1,4}$, respectively. This indicates that the total average pressure in this situation is a suboptimal combination of the four source regions.

A more uniform pressure distribution is obtained, as shown in part (b) of Fig. 5, when we keep the source density in $I_{s2,3}$ at its original level of 0.0084 but increase the density in regions, $I_{s1,4}$. In this case the maximum of calculated pressure in regions I_{s1} and I_{s4} is 610 Pa and slightly lower in regions I_{s2} and I_{s3}. Note that this is very close to the p_1 value of the one-dimensional case mentioned above.

The air flow vectors V corresponding to these cases are also given in Fig. 5. In both these cases the air flow is from high-pressure regions to low-pressure regions, as would be expected. We see that the flow direction is reversed by increasing the source density in the side regions. This situation indicates that the air flow from the side source areas $I_{s2,3}$ can be used to "block" the main air-flow coming from the larger areas $I_{s1,4}$.

In order to show this blocking effect several cases with different $\alpha_{2,3}$ and $\alpha_{1,4}$ values were evaluated for a constant total air inflow area $2l(\alpha_{2,3}(L_x - 2l) + \alpha_{1,4}L_y) = 0.0167$. Figure 6 shows the air velocity profiles for $\Gamma = \infty$ and $\Gamma = 3.8$, where Γ is the ratio of the air flow rate into the different source regions

$$\Gamma = \frac{q_4}{q_2} = \frac{L_y}{L_x - 2l} \left(\frac{\alpha_4}{\alpha_2} \right). \qquad (17)$$

The $\Gamma = \infty$ case has no holes in the side region, and the latter case has a uniform α value. When there are no holes in the side region the air can escape from the edges B_2 and B_3 with high velocity resulting in lower pressure. In contrast, when the side region has pressure holes the air flow in the no source region is reduced and the sources of the two regions are almost "separated" from each other. In this case the pressure generated in the mid region is higher. In order to evaluate the effect of the density distributions we use the average pressure p_{ave} obtained by dividing the numerically integrated two-dimensional pressure distribution by the total reverser area.

In fact, when we look at the effect of Γ on the average pressure, given in Fig. 7, we see that the maximum occurs at $\Gamma = 3.8$ (uniform α). In this case the pressure distribution on all four side regions is nearly identical. Thus very little pressure gradient exist to cause flow in the no-source region. Therefore, the average pressure attains the optimal value. This shows that, as the pressure in the no-source region is a function of the ratio $\alpha l/h$, *it is crucial to keep this ratio constant throughout the whole reverser surface, in order to optimize the average pressure in the clearance.*

5.3 The Effect of $\alpha l/h$ on Average Pressure. Figure 8 shows a plot of the average pressures as a function of the parameter $\alpha l/h$ calculated by the one-dimensional and two-dimensional solutions, an empirical relation and the air-jet the-
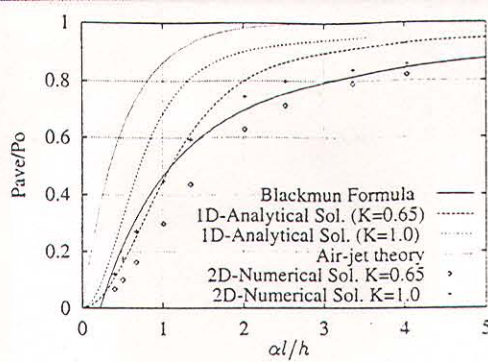
Fig. 8 Average pressure under the entire web as a function of dimensionless parameter $\alpha l/h$ ($\epsilon_o = 2.5 \times 10^{-2}$, $p_0 = 800$ Pa)

ory. A uniform α value was used in all four source domains for the two-dimensional calculations.

The average pressure for the one-dimensional solution over the entire web area is

$$p_{\text{ave}} = \left(1 - \frac{2l}{L_x}\right)p_1 + \left(\frac{2l}{L_x}\right)\bar{p}. \qquad (18)$$

where

$$\bar{p} = \frac{1}{l}\int_0^l p\,dx = p_0\left[1 - \frac{1 + \dfrac{\sinh(2m)}{2m}}{1 + \cosh(2m)}\right]. \qquad (19)$$

Blackmun's formula is a semi-empirical relation based on data for two-dimensional reversers with values of $\alpha l/h$ between about 0.4 and 1 given by

$$\bar{p} = p_0\left[1 - 1.24\,\frac{1 - e^{-2\alpha l/h}}{2\alpha l/h}\right] \qquad (20)$$

(Blackmun).

An analytical expression for the cushion pressure p_1 for the hovercraft is obtained by integrating the Euler's equations along and across the stream lines of the air jet when the pressure on the inside of the air jet is assumed to be p_1 and on the outside of the air-jet it is assumed to be the ambient pressure P_a,

$$p_1 = p_0(1 - e^{-2\chi}). \qquad (21)$$

Here p_0 is the supply pressure and $\chi = 2r_h/h$ when the jets are perpendicular to the ground (Elsley and Devereux, 1968). The diameter of the air-hole is given by $2r_h$. In Fig. 8 the air-jet Eq. (21) is used by assuming that $\chi = \alpha l/h$, (or $2r_h = \alpha l$).

Except for the air-jet formula, the results agree reasonably well. The two-dimensional solution is always lower than the one-dimensional solution due to the existence of the corner regions, where the actual pressure is lower than what the one-dimensional solution predicts. In the range $0 \leq \alpha l/h \leq 1$, both the one-dimensional and two-dimensional solutions for discharge coefficient $\kappa = 0.65$ predict lower average pressures than Blackmun's formula. If we increase κ to 1, the two-dimen-

sional solution agrees quite well with Blackmun's formula. This suggests that the effective discharge coefficient may be higher than 0.65. Further experimentation to determine the discharge coefficient might be warranted.

6 Summary and Conclusions

The equations governing the air flow in an air reverser are derived. The flow is averaged across the clearance, which is much smaller than the other dimensions of the problem; the resulting equations apply in the plane of the reverser. An analytical solution for the governing equations is found for the case in which the flow is one-dimensional and web-reverser gap is constant. Comparing this solution with the two-dimensional numerical solution shows that the flow is approximately one-dimensional along each edge, except near the corners. As a result of this, the average pressure under the web is overestimated by the one-dimensional solution. The parameter $\kappa \alpha l/h$, the ratio of the effective hole area to the total exit area, is the main factor in controlling the average pressure under the web: in general, increasing $\kappa \alpha l/h$ results in higher average pressure. Two-dimensional analysis of the problem showed that dissimilar hole densities in the source regions may cause air flow in the no-source region, leading to reductions in the average pressure and a nonuniform pressure distribution. The average pressure is maximized when the ratio $\kappa \alpha l/h$ is kept uniform on the outer periphery of the reverser surface.

References

Abramovich, G. N., 1963, *The Theory of Turbulent Jets*, M.I.T. Press, Cambridge, MA.

Blackmun, R. C., 1997, "Correlation of Factors Affecting Web Clearance Around Air Reversers," private communication. Eastman Kodak Company, Rochester, NY.

Burden, R. L., and Faires, J. D., 1989, *Numerical Analysis*, PWS-Kent, Boston.

Chandra, C. J. G., Srinivas, Y. L., Seetharamu, K. H., and Parameswaran, M. A., 1990, "Investigation of Air Film Conveyor Pressurised Through Multiple Holes," *Finite Elements in Analysis and Design*, Vol. 6. pp. 235–243.

Elsley, G. H., and Devereux, A. J., 1968, *Hovercraft Design and Construction*, Cornell Maritime Press, Cambridge, MD.

Fletcher, C. A. J., 1991, *Computational Techniques for Fluid Dynamics*, Springer-Verlag, Berlin.

Gerhart, P. M., Gross, R. J., and Hochstein, J. I., 1992, *Fundamentals of Fluid Mechanics*, Addison-Wesley, Reading, MA.

Gross, W. A., ed., 1980, *Fluid Film Lubrication*, John Wiley and Sons, New York.

Hamrock, B. J., 1994, *Fundamentals of Fluid Film Lubrication*, McGraw-Hill, New York.

Hirsch, C., 1988, *Numerical Computation of Internal and External Flows*, John Wiley and Sons, Chichester, UK.

Kwak, D., Chang, J. L. C., Shanks, S. P., and Chakravarthy, S. R., 1986, "A Three-Dimensional Incompressible Navier-Stokes Solver Using Primitive Variables," *AIAA Journal*, Vol. 24, No. 3, pp. 390–395.

Lewis, T. S., 1997, "The Fluid Dynamics of Air Reversers," private communication. Eastman Kodak Company, Rochester, NY.

Müftü, S., and Benson, R. C., 1996, "A Study of Cross-Width Variations in the Two Dimensional Foil Bearing Problem," ASME *Journal of Tribology*, Vol. 118, pp. 407–414.

Müftü, S., Lewis, T. S., and Cole, K. A., 1997, "A Numerical Solution of the Euler's Equations with Non-linear Source Terms in Modeling the Fluid Dynamics of an Air Reverser," *Proceedings of the Information Storage and Processing Systems Symposium*, ASME Winter Annual Meeting. Dallas, TX.

Pozzi, A., Manzo, F., and Luchini, P., 1993, "Compressible Flow in a Hovercraft Air Cushion," *AIAA Journal*, Vol. 31, No. 3, pp. 528–533.

Pulliam, T. H., 1985, "Artificial Dissipation Models for the Euler Equations," AIAA-85-0438.

Rajaratnam, N., 1976, *Turbulent Jets*, Elsevier Scientific Publishing Co., Amsterdam.